GLOBAL DYNAMICS OF THE HOŘAVA-LIFSHITZ COSMOLOGY WITH NON-ZERO CURVATURE

FABAO GAO[1,2], AND JAUME LLIBRE[2]

Abstract. The global dynamics of a cosmological model based on Hořava-Lifshitz gravity in the presence of curvature is described by using the qualitative theory of differential equations.

1. Introduction

In recent years Hořava [1] proposed a spacetime asymmetric gravitational theory similar to Lifshitz's scalar field theory, also known as Hořava-Lifshitz gravity. This theory has inspired a great deal of research for its applications in cosmology and black hole physics (see [2]-[17] or the review articles [18], [19] and the references therein).

Here we will investigate the global dynamics of the Hořava-Lifshitz scalar field cosmology under the Friedmann-Lemaître-Robertson-Walker background spacetime in the presence of curvature and no cosmological constant term. The corresponding dimensionless field equations admit the following form

$$\begin{aligned} \frac{dx}{dt} &= x\left(3x^2-2z^2-3\right)+\sqrt{6}s\left(1-x^2+z^2\right), \\ \frac{dz}{dt} &= z\left(3x^2-2z^2-2\right), \\ \frac{ds}{dt} &= -2\sqrt{6}xf(s), \end{aligned} \tag{1}$$

Key words and phrases. Hořava-Lifshitz; Global dynamics; Cosmology; Poincaré compactification.

where the power law potential $f(s) = -s^2/(2n)$ with a natural number n. See equations equations (113)-(115) of [8] or (44)-(46) of [14] for more details.

The Hořava-Lifshitz cosmological model with zero curvature and without cosmological constant term was studied in [5]. Furthermore, in the references [3, 7, 8, 9, 14], the authors either studied the global dynamics of the planar case of system (1) considering only the variables x and z by using the two-dimensional Poincaré compactification, or discussed only local dynamics of system (1) without investigate the dynamics close to infinity. Our study fully describes the global dynamics of system (1) in the region $G = \{(x, z, s) \in \mathbb{R}^3 : x^2 - z^2 \leq 1\}$ of physical interest.

2. Phase portraits on the invariant planes and surface

In order to study the local phase portraits of the finite and infinite equilibrium points, and the global phase portraits of system (1) in the region G, which is the meaningful region for cosmology, see again [8] or [14]. We start discussing the phase portraits on its invariant planes and surface

$$z = 0,\ s = 0,\ x^2 - z^2 = 1.$$

2.1. The invariant plane $z = 0$.

On this plane system (1) becomes

$$\begin{aligned} \frac{dx}{dt} &= (x^2 - 1)\left(3x - \sqrt{6}s\right), \\ \frac{ds}{dt} &= \frac{\sqrt{6}}{n}\, x s^2. \end{aligned} \tag{2}$$

The phase portraits of system (2) in the strip $z = 0$ and $x^2 - z^2 \leq 1$, i.e. in $z = 0,\ -1 \leq x \leq 1$, it has been studied in [5], and the phase

portraits is shown in Figure 1, where the hyperbolic equilibrium point $e_0 = (0, 0)$ is a saddle, both the semi-hyperbolic equilibrium points $e_1 = (1, 0)$ and $e_2 = (-1, 0)$ are saddle-nodes.

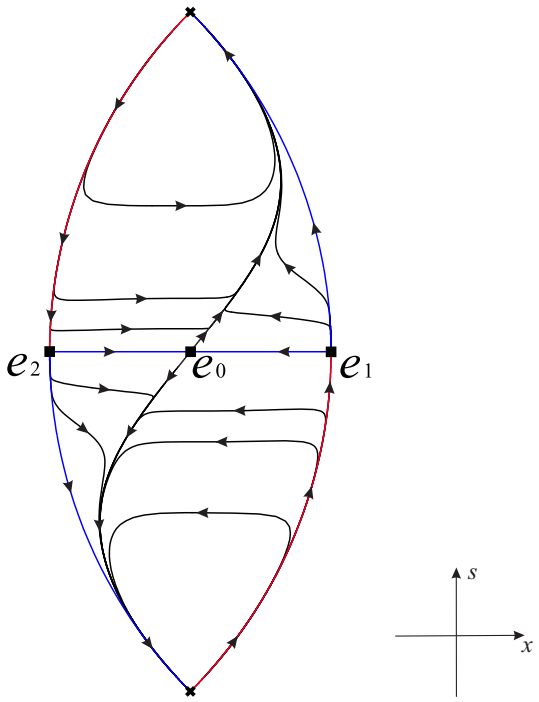

FIGURE 1. The phase portraits of the invariant plane $z = 0$ in the region $-1 \leq x \leq 1$.

2.2. **The invariant plane $s = 0$.** On this plane system (1) becomes

$$\frac{dx}{dt} = x\left(3x^2 - 2z^2 - 3\right), \ \frac{dz}{dt} = z\left(3x^2 - 2z^2 - 2\right), \tag{3}$$

which has three equilibrium points $e_0 = (0, 0)$, $e_1 = (1, 0)$ and $e_2 = (-1, 0)$. Here e_0 is a hyperbolic stable node with eigenvalues -3 and -2, both e_1 and e_2 are unstable hyperbolic nodes with eigenvalues 6 and 1.

On the local chart U_1 (see Chapter 5 of [20] for more details on the Poincaré compactification) system (3) becomes

$$\frac{du}{dt} = uv^2, \ \frac{dv}{dt} = v\left(-3 + 2u^2 + 3v^2\right). \tag{4}$$

Since this system vanishes at $v = 0$, all the points at infinity are equilibrium points. Taking the transformation with respect to time $d\tau = vdt$ yields

$$\frac{du}{d\tau} = uv, \ \frac{dv}{d\tau} = -3 + 2u^2 + 3v^2. \tag{5}$$

This system has two hyperbolic points at infinity, $e_3 = (-\sqrt{6}/2, 0)$ and $e_4 = (\sqrt{6}/2, 0)$, both of them are unstable hyperbolic saddle points with eigenvalues $\pm\sqrt{6}$.

On the local chart U_2 system (3) writes

$$\frac{du}{dt} = -uv^2, \ \frac{dv}{dt} = v\left(2 - 3u^2 + 2v^2\right). \tag{6}$$

Rescaling the time of system (6) by letting $d\tau = vdt$ we obtain

$$\frac{du}{d\tau} = -uv, \ \frac{dv}{d\tau} = 2 - 3u^2 + 2v^2. \tag{7}$$

In view of $(0, 0)$ is not an equilibrium point of system (7), we will not continue to study other infinite equilibrium points of system (7) because they have been studied in local chart U_1.

Therefore the global phase portraits of system (3) can be found in Figure 2.

2.3. **The invariant surface $x^2 - z^2 = 1$.** First we prove that the surface $x^2 - z^2 = 1$ is invariant under the flow of system (1). If $l = l(x, z, s) = x^2 - z^2 - 1$, then in order that the surface $x^2 - z^2 = 1$ be

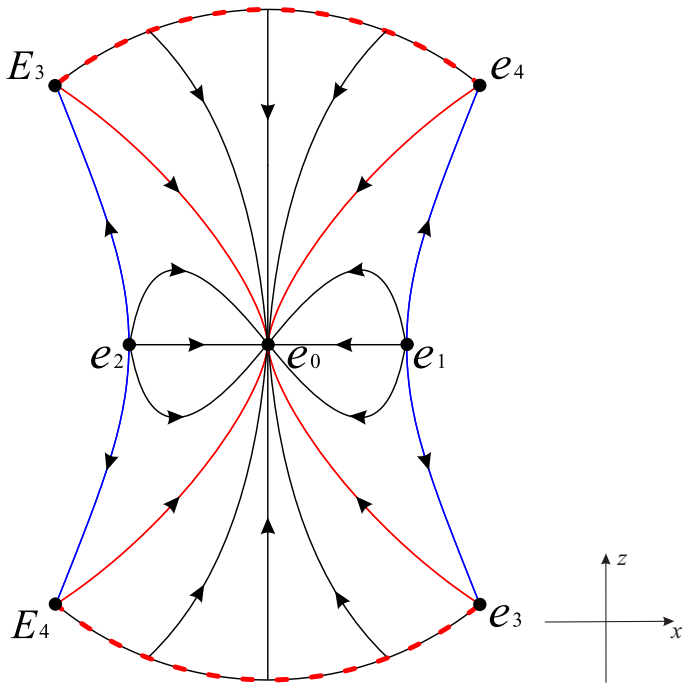

FIGURE 2. The phase portrait on the invariant plane $s = 0$ restricted to the region $x^2 - z^2 \leq 1$.

invariant we must have

$$\frac{\partial l}{\partial x}\dot{x} + \frac{\partial l}{\partial z}\dot{z} + \frac{\partial l}{\partial s}\dot{s} = Kl,$$

for some polynomial K, and this is the case with $K = 2(3x^2 - 2z^2 - \sqrt{6}xs)$.

On the surface $x^2 - z^2 = 1$ system (1) can be written as

$$\frac{dx}{dt} = x\left(x^2 - 1\right), \quad \frac{ds}{dt} = \frac{\sqrt{6}}{n}xs^2. \tag{8}$$

Then except for all the points on $x = 0$ which are equilibrium points, system (8) also admits two finite equilibrium points $e_1 = (1, 0)$ and $e_2 = (-1, 0)$. By using Theorem 2.19 of [20], we can find that both e_1 and e_2 are semi-hyperbolic saddle-nodes.

On the local chart U_1 system (8) becomes

$$\frac{du}{dt} = u\left(\frac{\sqrt{6}}{n}u + v^2 - 1\right),\ \frac{dv}{dt} = v\left(v^2 - 1\right). \tag{9}$$

It has two infinite equilibrium points $e_5 = (0, 0)$ and $e_6 = (\sqrt{6}n/6, 0)$, where e_5 is a hyperbolic stable node with eigenvalues -1 of multiplicity two, and e_6 is a hyperbolic unstable saddle point with eigenvalues ± 1.

On the local chart U_2 system (8) writes

$$\frac{du}{dt} = u\left(-\frac{\sqrt{6}}{n}u + u^2 - v^2\right),\ \frac{dv}{dt} = -\frac{\sqrt{6}}{n}uv. \tag{10}$$

Let $d\tau = udt$ we obtain

$$\frac{du}{d\tau} = -\frac{\sqrt{6}}{n}u + u^2 - v^2,\ \frac{dv}{d\tau} = -\frac{\sqrt{6}}{n}v. \tag{11}$$

The origin $e_7 = (0, 0)$ on the local chart U_2 is a hyperbolic stable node with eigenvalues $-\sqrt{6}/n$ of multiplicity two.

In short the global phase portraits of system (8) is shown in Figure 3.

2.4. **The finite equilibrium points.** It is noted that system (1) admits three finite equilibrium points $p_0 = (0, 0, 0)$ with eigenvalues $(-3, -2, 0)$, $p_1 = (1, 0, 0)$ and $p_2 = (-1, 0, 0)$ with the same eigenvalues $(6, 1, 0)$. Here p_1 and p_2 are located at the intersection of the invariant planes $z = 0$, $s = 0$ and the invariant surface $x^2 - z^2 = 1$, corresponding to the equilibrium points e_1 and e_2 in subsections 2.1-2.3, respectively. The origin p_0 of system (1) lies at the intersection of the invariant planes $z = 0$ and $s = 0$, which is the same point as the equilibrium point e_0 studied in subsections 2.1 and 2.2.

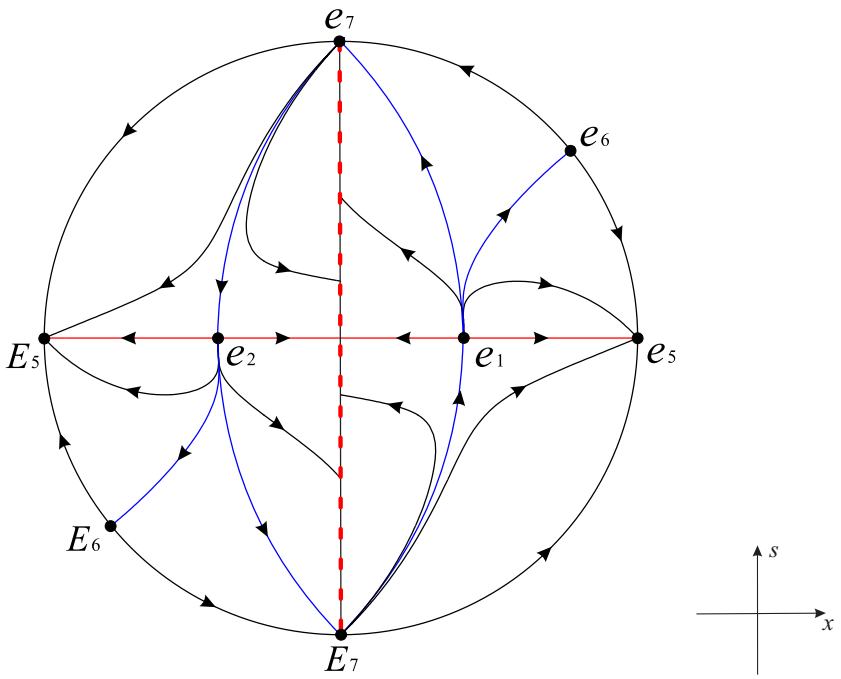

FIGURE 3. The phase portrait of the invariant surface $x^2 - z^2 = 1$.

3. Phase portraits on the Poincaré sphere at infinity

In order to describe the dynamics of system (1) at infinity. We use the method of the three-dimensional Poincaré compactification (see [21] for more details) $x = 1/z_3,\ z = z_1/z_3,\ s = z_2/z_3$, then the analytical vector field of system (1) on the local chart U_1 becomes

$$
\begin{aligned}
\frac{dz_1}{dt} &= z_1\left[z_3^2 - \sqrt{6}z_2\left(-1 + z_1^2 + z_3^2\right)\right], \\
\frac{dz_2}{dt} &= z_2\left[-3 + 2z_1^2 + 3z_3^2 + \sqrt{6}z_2\left(\frac{1}{n} + 1 - z_1^2 - z_3^2\right)\right], \\
\frac{dz_3}{dt} &= -z_3\left[z_1^2\left(-2 + \sqrt{6}z_2\right) + \left(-3 + \sqrt{6}z_2\right)\left(-1 + z_3^2\right)\right].
\end{aligned} \tag{12}
$$

In the different local charts of the Poincaré sphere, the infinity of $\mathbb{R}^3$ corresponds to $z_3 = 0$, then system (12) has the equilibrium points listed in Table 1. Except that the equilibrium point u_{31} denotes the

origin of the local chart U_3, the rest equilibrium points lie in the local chart U_1. Moreover the straight line $s = 0$ of the local chart U_1 is filled with the equilibrium points u_{a0} for all $a \in \mathbb{R}$.

TABLE 1. Equilibrium points on the different local charts of the Poincaré sphere at the infinity of $\mathbb{R}^3$.

Equilibrium points	**Eigenvalues**
$u_{11} = (0, 0, 0)$	$(-3, -3, 0)$
$u_{12} = \left(-\frac{\sqrt{6}}{2}, 0, 0\right)$	$(0, 0, 0)$
$u_{13} = \left(\frac{\sqrt{6}}{2}, 0, 0\right)$	$(0, 0, 0)$
$u_{14} = \left(-1, \frac{\sqrt{6}}{6}n, 0\right)$	$(-1, 1, -2n)$
$u_{15} = \left(1, \frac{\sqrt{6}}{6}n, 0\right)$	$(-1, 1, -2n)$
$u_{16} = \left(0, \frac{\sqrt{6}}{2}\frac{n}{1+n}, 0\right)$	$\left(-\frac{3}{1+n}, \frac{3n}{1+n}, 3\right)$
$u_{a0} = (a, 0, 0)$	$\left(0, -3+2a^2, -3+2a^2\right)$
$u_{31} = (0, 0, 0)$	$(0, 0, 0)$

For the case $z_3 = 0$ system (12) is reduced to

$$\begin{aligned} \frac{dz_1}{dt} &= -\sqrt{6}z_1 z_2 \left(-1 + z_1^2\right), \\ \frac{dz_2}{dt} &= z_2 \left[-3 + 2z_1^2 + \sqrt{6}z_2 \left(\frac{1}{n} + 1 - z_1^2\right)\right]. \end{aligned} \tag{13}$$

After changing the of time $d\tau = z_2 dt$ system (13) becomes

$$\begin{aligned} \frac{dz_1}{d\tau} &= -\sqrt{6}z_1 \left(-1 + z_1^2\right), \\ \frac{dz_2}{d\tau} &= -3 + 2z_1^2 + \sqrt{6}z_2 \left(\frac{1}{n} + 1 - z_1^2\right). \end{aligned} \tag{14}$$

Then this system has three equilibrium points $e_{i,1}$, $e_{i,2}$ and $e_{i,3}$ with coordinates $(-1, \sqrt{6}n/6)$, $(1, \sqrt{6}n/6)$ and $(0, \sqrt{6}n/(2(1+n)))$, respectively. Here both $e_{i,1}$ and $e_{i,2}$ are unstable saddle points with eigenvalues $\sqrt{6}/n$ and $-2\sqrt{6}$. $e_{i,3}$ is an unstable node with eigenvalues $\sqrt{6}$ and $\sqrt{6}(1+n)/n$. The phase portrait on the Poincaré sphere at infinity on local chart U_1 is shown in Figure 4.

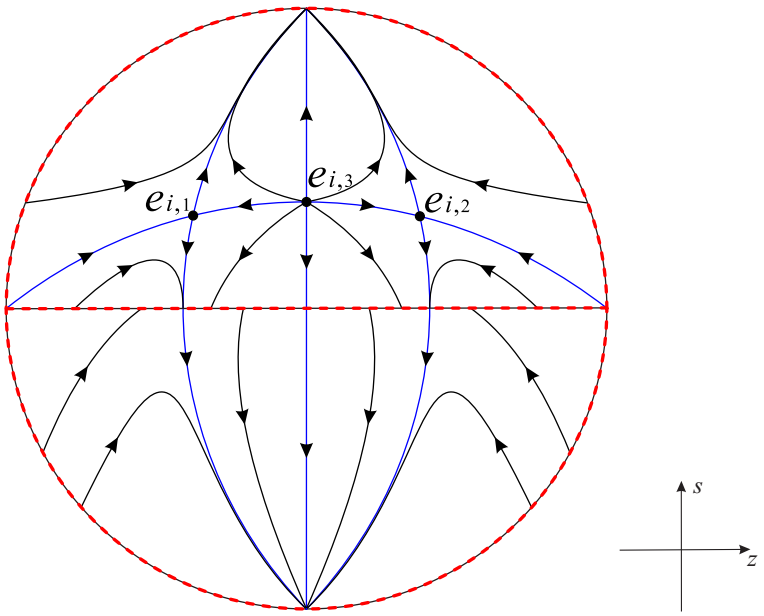

FIGURE 4. The phase portrait of system (1) at infinity on local chart U_1.

On the local chart U_2 in view of Poincaré compactification $x = z_1/z_3$, $z = 1/z_3$, $s = z_2/z_3$, system (1) writes

$$
\begin{aligned}
\frac{dz_1}{dt} &= -z_1 z_3^2 + \sqrt{6} z_2 \left(1 - z_1^2 + z_3^2\right), \\
\frac{dz_2}{dt} &= z_2 \left(2 - 3z_1^2 + \frac{\sqrt{6}}{n} z_1 z_2 + 2z_3^2\right), \\
\frac{dz_3}{dt} &= z_3 \left(2 - 3z_1^2 + 2z_3^2\right).
\end{aligned} \tag{15}
$$

Since we want to study the infinity we take $z_3 = 0$, rescaling the time $d\tau = z_2 dt$ system (15) is equivalent to

$$\begin{aligned} \frac{dz_1}{d\tau} &= \sqrt{6}\,(1 - z_1^2)\,, \\ \frac{dz_2}{d\tau} &= 2 - 3z_1^2 + \frac{\sqrt{6}}{n} z_1 z_2. \end{aligned} \tag{16}$$

For any constant b, since $(b, 0)$ is not the equilibrium point of the system (16), we will not continue to discuss other infinite equilibrium points of the system (16). Because this has been discussed in the case U_1.

On the local chart U_3 the three-dimensional Poincaré compactification is $x = z_1/z_3,\ z = z_2/z_3,\ s = 1/z_3$, then system (1) becomes

$$\begin{aligned} \frac{dz_1}{dt} &= z_1 \left[-\frac{\sqrt{6}(1+n)}{n} z_1 + 3z_1^2 - 2z_2^2 - 3z_3^2 \right] + \sqrt{6}\,(z_2^2 + z_3^2)\,, \\ \frac{dz_2}{dt} &= z_2 \left[-\frac{\sqrt{6}}{n} z_1 + 3z_1^2 - 2\,(z_2^2 + z_3^2) \right], \\ \frac{dz_3}{dt} &= -\frac{\sqrt{6}}{n} z_1 z_3. \end{aligned} \tag{17}$$

For the case $z_3 = 0$ from system (17) we obtain

$$\begin{aligned} \frac{dz_1}{dt} &= z_1 \left[-\frac{\sqrt{6}(1+n)}{n} z_1 + 3z_1^2 - 2z_2^2 \right] + \sqrt{6} z_2^2, \\ \frac{dz_2}{dt} &= z_2 \left(-\frac{\sqrt{6}}{n} z_1 + 3z_1^2 - 2z_2^2 \right). \end{aligned} \tag{18}$$

It is noted that $(0, 0)$ is a linearly zero equilibrium point, the topological index is zero from the Poincaré-Hopf theory (see Theorem 6.30 of [20] for more details). In order to study its local phase portrait we shall use vertical blow-ups (see for instance [22]) by letting $w = z_2/z_1$, then

we obtain

$$
\begin{aligned}
\frac{dz_1}{dt} &= z_1^2\left[\sqrt{6}\left(-\frac{1}{n}-1+w^2\right)+\left(3-2w^2\right)z_1\right], \\
\frac{dw}{dt} &= -\sqrt{6}z_1 w\left(-1+w^2\right).
\end{aligned} \tag{19}
$$

Eliminating the common factor z_1 of system (19) by changing the time $d\tau = z_1 dt$ it yields

$$
\begin{aligned}
\frac{dz_1}{d\tau} &= z_1\left[\sqrt{6}\left(-\frac{1}{n}-1+w^2\right)+\left(3-2w^2\right)z_1\right], \\
\frac{dw}{d\tau} &= -\sqrt{6}w\left(-1+w^2\right).
\end{aligned} \tag{20}
$$

System (20) admits three equilibrium points $e_{i,4} = (0,-1)$, $e_{i,5} = (0,1)$ and $e_{i,6} = (0,0)$ on $z_1 = 0$, where $e_{i,4}$ and $e_{i,5}$ are two hyperbolic stable nodes with eigenvalues $-\sqrt{6}/n$ and $-2\sqrt{6}$, $e_{i,6}$ is a hyperbolic unstable saddle point with eigenvalues $\sqrt{6}$ and $-\sqrt{6}(1+n)/n$. The local phase portraits around $e_{i,4}$, $e_{i,5}$ and $e_{i,6}$ are shown in Figure 5(a). Note that there is a time rescaling $d\tau = z_1 dt$ between systems (19) and (20), so the direction of the trajectories in the local phase portraits of system (19) is opposite to that of Figure 5(a) when $z_1 < 0$, see Figure 5(b) for more details. In addition, all points on the w axis, i.e. $z_1 = 0$, are singularities of system (19). Thus the local phase portraits at $(0,0)$ of system (18) is shown in Figure 5(c). Then the phase portrait in the local chart U_3 is shown in Figure 6.

In summary joining the previous information we obtain the global phase portraits at infinity in the Poincaré sphere in Figure 7.

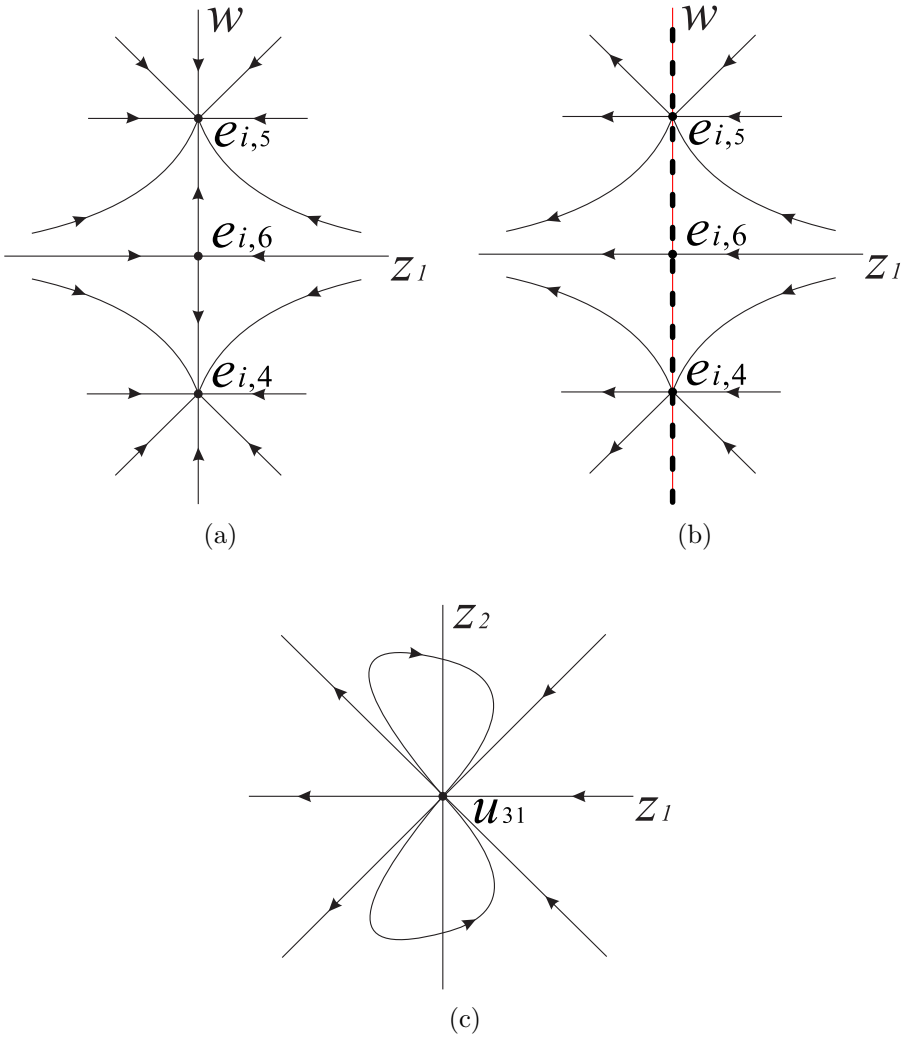

FIGURE 5. In (a), (b) and (c) there are the local phase portraits of the equilibrium points in systems (20), (19) and (18), respectively.

4. Phase portraits inside the Poincaré ball restricted to $x^2 - z^2 \leq 1$

It is noted that system (1) is invariant under the symmetries $(x, z, s) \mapsto (-x, -z, -s)$ and $(x, z, s) \mapsto (-x, z, -s)$, so it is invariant under the

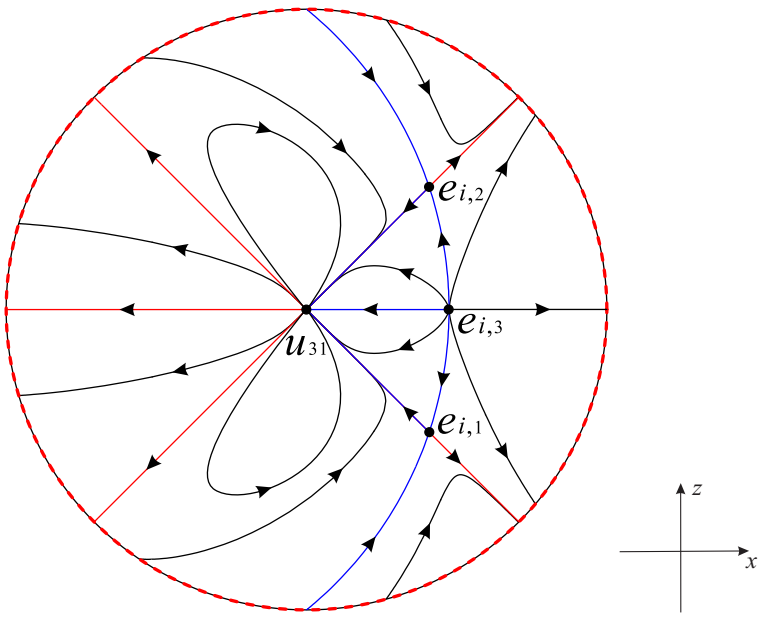

FIGURE 6. The phase portrait of system (18), i.e. the phase portrait at infinity in the local chart U_3 of system (1).

symmetry with respect to the origin and to the z-axis. Now we divide the Poincaré ball restricted to $x^2 - z^2 \leq 1$ into the following four regions:

$$R_1 : \ z \leq 0, \ s \geq 0. \quad R_2 : \ z \leq 0, \ s \leq 0.$$
$$R_3 : \ z \geq 0, \ s \geq 0. \quad R_4 : \ z \geq 0, \ s \leq 0.$$

Then due to the symmetries we only need to study the phase portraits of system (1) in the region R_1.

Combining the phase portraits of the invariant surface $x^2 - z^2 = 1$ with the phase portraits of the planes $z = 0$, and $s = 0$, together with the phase portrait at infinity, we get the phase portraits on the boundary of the region R_1 as shown in Figures 8-10. Here we explain the definition of the three-dimensional cartesian coordinate system in this paper as follows: we regard the xz-plane as the horizontal plane

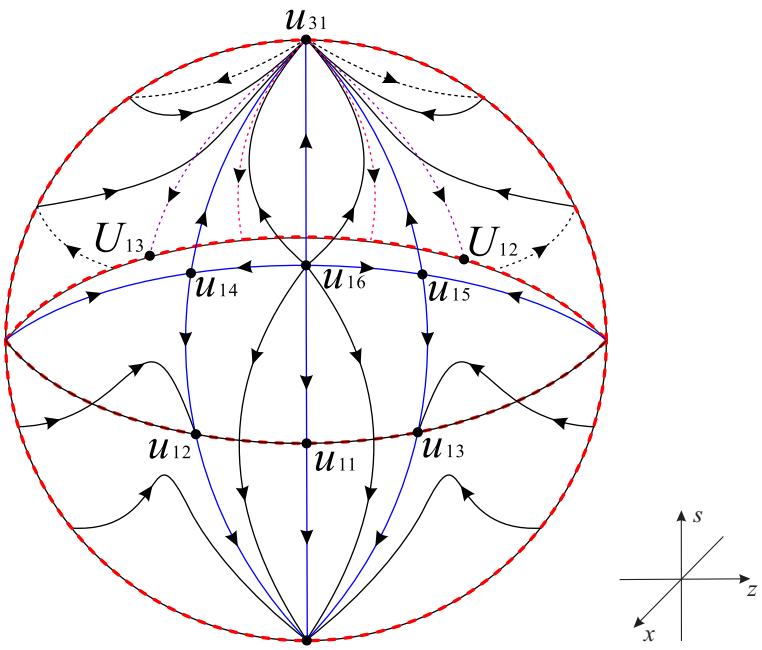

FIGURE 7. The global phase portrait at infinity in the Poincaré sphere. The North Pole of the Poincaré ball is the equilibrium point u_{31}. The symmetric points of u_{12} and u_{13} with respect to the center of the sphere are U_{12} and U_{13}, respectively.

in $\mathbb{R}^3$, where the direction of the z-axis is horizontal towards the right. If the z-axis axis rotates 90 degrees clockwise we get the x-axis. The s-axis is vertical upward, and then xzs constitutes a three-dimensional right-handed cartesian coordinate system.

In order to show the phase portraits more clearly, the boundary of the region R_1 is divided into six surfaces according to the orientation towards us, the back to us and the bottom area. See Figure 11 for more details. It is noted that the North Pole u_{31} of the Poincaré ball on the front boundary surfaces F_1 and F_2 is stable, and there is an elliptic sector and a stable parabolic sector segment of U_3 on the boundary F_3, but it is unstable on the back boundary surfaces B_1 and B_2.

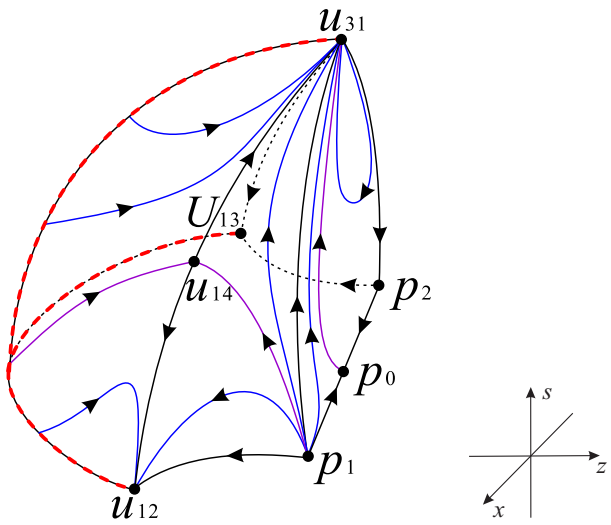

FIGURE 8. Phase portrait in the front boundary of the region R_1.

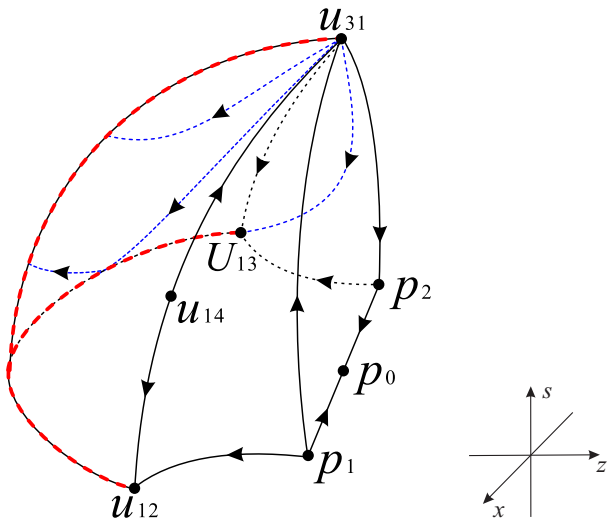

FIGURE 9. Phase portrait in the back boundary of the region R_1.

5. Dynamics in the interior of the region R_1

Note that the original system (1) admits the three finite equilibrium points p_0, p_1 and p_2 in the three-dimensional cartesian coordinate

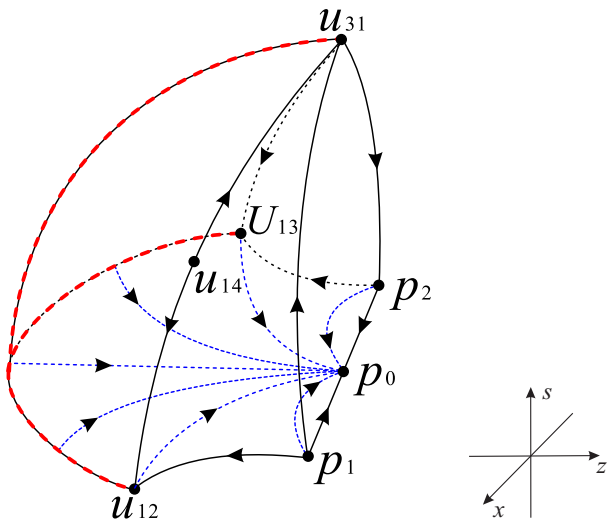

FIGURE 10. Phase portrait in the bottom of the region R_1.

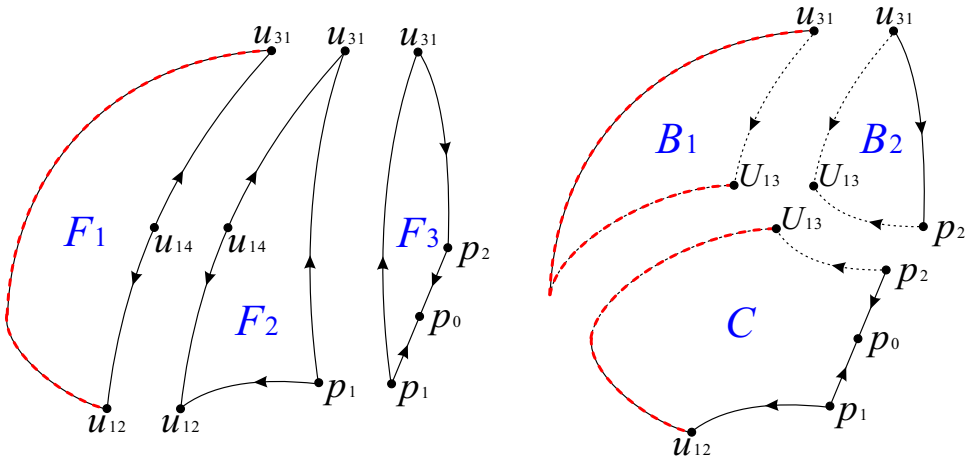

FIGURE 11. The six boundary surfaces of the region R_1.

system. The dynamical behavior of the system inside the region R_1 depends on the behavior of the flow in the following surfaces and planes

$$h(x,z,s)=0,\ g(x,z)=0,\ x=0,\ z=0,\ s=0,$$

where

$$\begin{aligned} h(x,z,s) &= x\left(3x^2-2z^2-3\right)+\sqrt{6}s\left(1-x^2+z^2\right), \\ g(x,z) &= 3x^2-2z^2-2. \end{aligned}$$

These surfaces and planes divide the region R_1 into seven different subregions $R_{1i},\ i=(1,2,\ldots,7)$, see Figures 12-19 for more details. It should be noted that R_{11} and R_{13} represent parallel tunnels inside R_1, respectively. It is easy to verify that $h>0$ in the subregions R_{12}, R_{14}, R_{15} and R_{16}, and $h<0$ in the subregions R_{11}, R_{13} and R_{17}. Similarly, we can find that $g>0$ in the subregions R_{11}, R_{12}, R_{16} and R_{17}, and $g<0$ in the subregions R_{13}, R_{14} and R_{15}. It should be noted that the dotted and solid lines in Figures 13-19 are consistent with those in Figure 12.

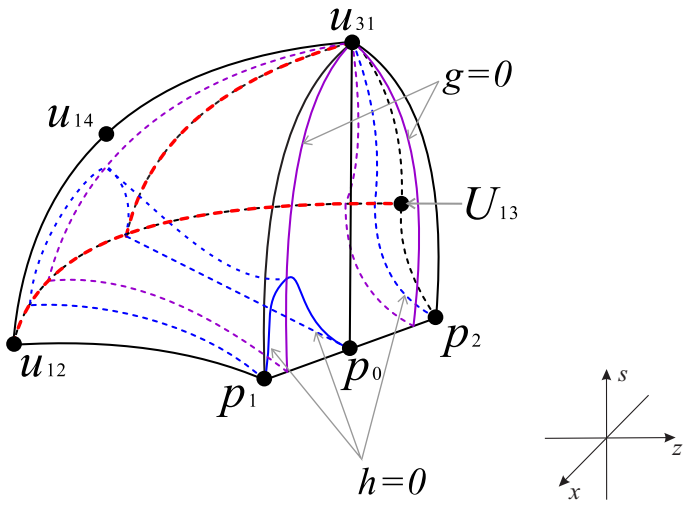

FIGURE 12. There are seven subregions inside the region R_1 of the Poincaré ball.

As shown in the subregion R_{11} (see Figure 13) the front surface consists of three dashed lines and one solid line contained in the surface

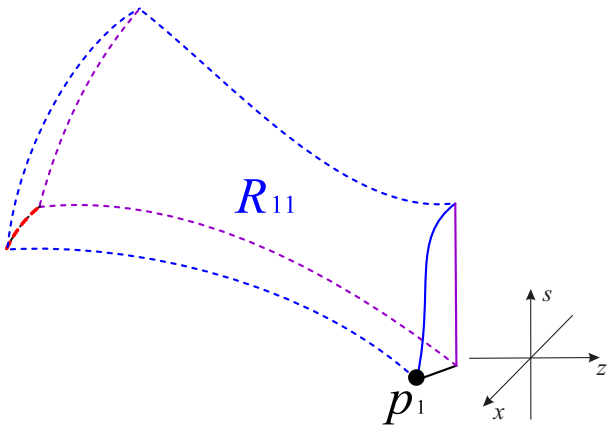

FIGURE 13. The subregion R_{11}.

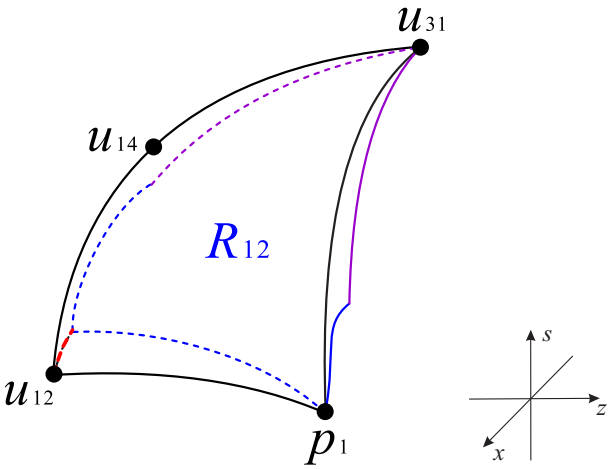

FIGURE 14. The subregion R_{12}.

$h = 0$, and the surface on the back side (opposite to the above front surface) contained in the surface $g = 0$.

In Table 2 we describe the behavior of $\dot{x}$, $\dot{z}$ and $\dot{s}$ in the seven subregions $R_{11}, \ldots, R_{17}$. From this table we obtain that the variables x and z in the subregion R_{11} decrease monotonically, and the variable s increases monotonically, so an orbit in the subregion R_{11} either crosses the boundary $h = 0$ and enters into the subregion R_{12}, or crosses the

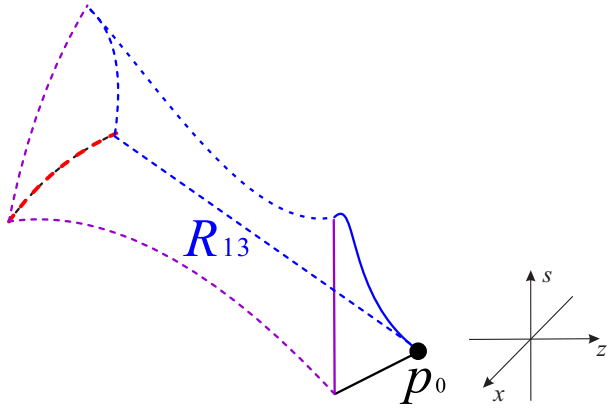

FIGURE 15. The subregion R_{13}.

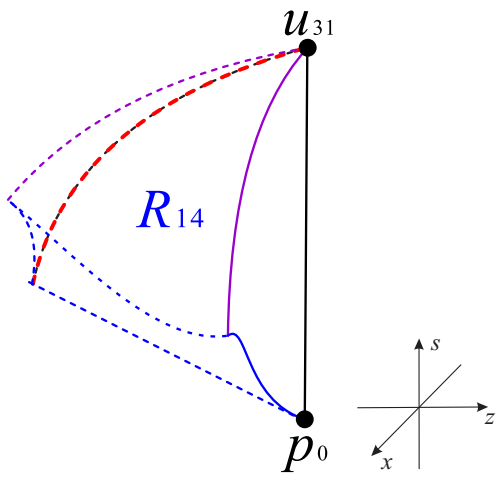

FIGURE 16. The subregion R_{14}.

boundary $g = 0$ and goes to the subregion R_{13}, or crosses the intersection curve of the subregions R_{11}, R_{12} and R_{13} into the subregion R_{14} with very low probability, i.e. an orbit in the subregion R_{11} will not stay in the future in this region, but will exit through its boundaries into other subregions, and these orbits in backwards time come from the equilibrium point p_1 in the subregion R_{11}. This process can be

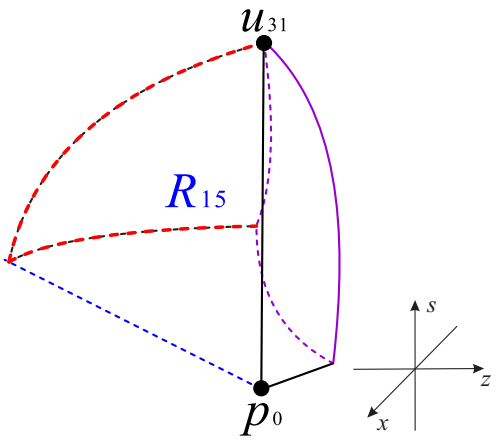

FIGURE 17. The subregion R_{15}.

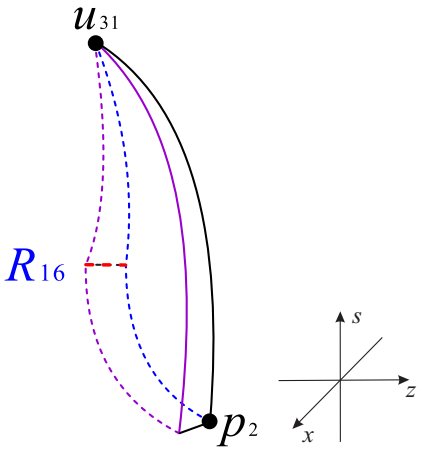

FIGURE 18. The subregion R_{16}.

simply summarized as follows

$$p_1 \longrightarrow R_{11} \longrightarrow R_{13}.$$
$$R_{11} \nearrow R_{12}$$
$$R_{11} \searrow R_{14}$$

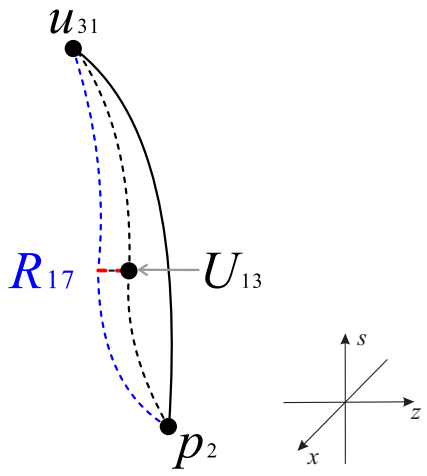

FIGURE 19. The subregion R_{17}.

TABLE 2. Dynamical behavior in seven different subregions

Subregions	**Corresponding Region**	**Increase or decrease**
R_{11}	$h<0,\ g>0,\ x>0,\ z<0,\ s>0$	$\dot{x}<0,\ \dot{z}<0,\ \dot{s}>0$
R_{12}	$h>0,\ g>0,\ x>0,\ z<0,\ s>0$	$\dot{x}>0,\ \dot{z}<0,\ \dot{s}>0$
R_{13}	$h<0,\ g<0,\ x>0,\ z<0,\ s>0$	$\dot{x}<0,\ \dot{z}>0,\ \dot{s}>0$
R_{14}	$h>0,\ g<0,\ x>0,\ z<0,\ s>0$	$\dot{x}>0,\ \dot{z}>0,\ \dot{s}>0$
R_{15}	$h>0,\ g<0,\ x>0,\ z<0,\ s>0$	$\dot{x}>0,\ \dot{z}>0,\ \dot{s}<0$
R_{16}	$h>0,\ g>0,\ x>0,\ z<0,\ s>0$	$\dot{x}>0,\ \dot{z}<0,\ \dot{s}<0$
R_{17}	$h<0,\ g>0,\ x>0,\ z<0,\ s>0$	$\dot{x}<0,\ \dot{z}<0,\ \dot{s}<0$

The front boundary of R_{12} (see Figure 14), i.e. the surface containing the equilibrium points u_{12}, u_{14}, u_{31} and p_1, is contained in the invariant surface $x^2 - z^2 = 1$ $(x > 0)$. The surface on the back side of R_{12} that contains the equilibrium points p_1 and u_{31} consists of two parts: the upper part surface containing the infinite equilibrium point u_{31} is the intersection of the subregions R_{12} and R_{14}, which is contained in the

surface $g = 0$, and the lower part surface containing the finite equilibrium point p_1, is the intersection of subregions R_{11} and R_{12} that is contained in the surface $h = 0$. The equilibrium points in the subregion R_{12} are the finite equilibrium point p_1, the infinite equilibrium points on the Poincaré sphere at $s = 0$ and the equilibrium point u_{14} at infinity. However an orbit in the subregion R_{12} does not start from these infinite equilibrium points at $s = 0$ or return to these points, but it comes from the finite equilibrium point p_1 or from the subregions R_{11} and R_{14} which have common boundaries with the subregion R_{12}. This is due to the fact that the variable z is decreasing monotonically and the variables x and s are increasing monotonically inside the subregion R_{12} according to Table 2. Moreover a trajectory in the subregion R_{12} will tend to the equilibrium point u_{14} at infinity. In summary, this dynamic behavior process can be represented as

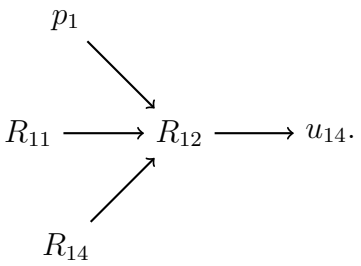

In the subregion R_{13} (see Figure 15) the front surface composed of three dashed lines and one solid line is contained in the surface $g = 0$, and its opposite surface is contained in the surface $h = 0$. From Table 2 an orbit in the subregion R_{13} may only comes from the equilibrium points locate at the infinity on $s = 0$ in R_{13}, or it comes from the subregions R_{11}. Then the orbit passes through the intersection of subregions R_{13} and R_{14} (contained in the surface $h = 0$) and enters

the subregion R_{14}, or tends to the infinite equilibrium point u_{31}, i.e. lies in the North Pole of the Poincaré sphere. So we obtain the following dynamics

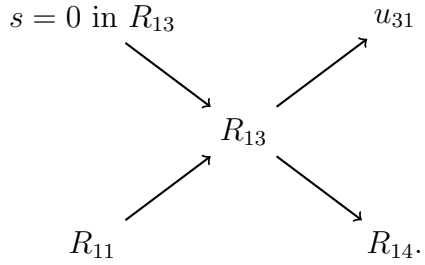

In subregion R_{14} (see Figure 16) the front triangular surface is contained in $g = 0$, and its opposite triangular surface is on the back side, which is included in the plane $x = 0$. According to Table 2 an orbit of the subregion R_{14} may come from the infinite equilibrium points on $x = 0$, or come from the subregion R_{13} through the surface $h = 0$, or from subregion R_{15} traversing plane $x = 0$, then go through the surface $g = 0$ into the subregion R_{12}, or directly goes to the infinite equilibrium point u_{31} at the North Pole of the Poincaré sphere. This can be represented as

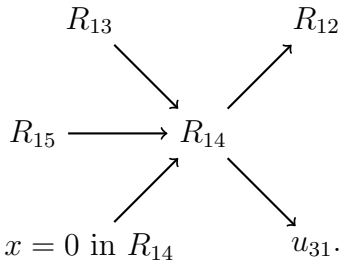

It can be noted from Figure 17 that the surface on the left of subregion R_{15} (consisting of two dashed lines and one solid line) is contained in plane $x = 0$, and the opposite surface to it is included in the surface $g = 0$. According to Table 2 an orbit in the subregion R_{15} can only come from the adjacent subregion R_{16}, and then either enter into the

subregion R_{14} adjacent to it, or directly tend to the finite equilibrium point p_0 located at the center of the Poincaré ball. This dynamics can be denoted as

$$R_{16} \longrightarrow R_{15} \begin{cases} \nearrow R_{14} \\ \searrow p_0. \end{cases}$$

We observe that the curved surfaces of the left and right sides of the subregion R_{16} (see Figure 18) are contained in the surfaces $g = 0$ and $h = 0$, respectively. It is known from Table 2 that an orbit in the subregion R_{16} can only come from the subregion R_{17} and crossing the surface $g = 0$, it enters into the subregion R_{15}. Thus we get that

$$R_{17} \longrightarrow R_{16} \longrightarrow R_{15}.$$

The left and right surfaces of subregion R_{17} (see Figure 19) are included in the surface $h = 0$ and in the invariant surface $x^2 - z^2 = 1$ ($x < 0$), respectively. According to Table 2, it is known that all three variables in subregion R_{17} are decreasing monotonically, so an orbit in this subregion must come from the infinite equilibrium point u_{31} located at the North Pole of Poincaré sphere and eventually tends to the infinite equilibrium point U_{13} in the invariant plane $s = 0$. Then we have that

$$u_{31} \longrightarrow R_{17} \longrightarrow U_{13}.$$

The dynamic behavior of the orbits inside the seven subregions of R_1 discussed above can be summarized as

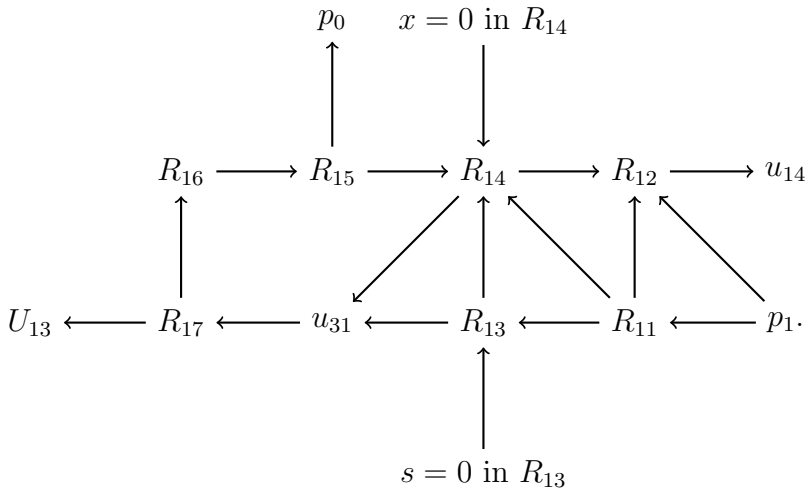

The above flow chart shows that the orbits of system (1) contained in the interior of the region R_1 have α-limit at the finite equilibrium point p_1, and the some orbits on the boundary of the region R_1 have α-limit at the $x = 0$ in R_{14}, or $s = 0$ in R_{13}. Moreover the orbits have ω-limit either at the finite equilibrium point p_0, or at the infinite equilibrium points u_{14} and U_{13}, where u_{14} is located on the intersection curve of the Poincaré sphere and the invariant surface $x^2 - z^2 = 1$ $(x > 0)$ at infinity, and U_{13} is located on the intersection of the Poincaré sphere and the invariant surfaces $s = 0$, $x^2 - z^2 = 1$ $(x < 0)$ at infinity (see Figure 12). Furthermore the orbits of system (1) on the boundary of R_1 also have α-limit and ω-limit at the infinite equilibrium point u_{31}, i.e. the North Pole of the Poincaré sphere.

In this way the qualitative global dynamic behavior of system (1) is described.

6. Discussion and conclusions

The physical meaning of the variables x, z and s in this paper can be found in references [3, 7, 8, 9, 14]. So we have

$$x = \frac{\dot{\phi}}{2\sqrt{6}H}, \quad z = \frac{\mu}{4(3\lambda-1)a^2H} \quad s = -\frac{V'(\phi)}{V(\phi)}, \tag{21}$$

where λ is a dimensionless constant, $V(\phi)$ is the potential, μ is a constant, and $H = \dot{a}/a$ is the Hubble parameter, and a is the dimensionless scale factor for the expanding universe.

Near infinity we note that the phase portrait described in Figure 2 has been obtained in [9], where the phase portrait of system (1) is limited to $s = 0$. Now we have completely described the phase portrait of system (1) with all s values in the region G as shown in Figures 8-10 and 12. By using the fact that system (1) remains invariant under two aforementioned symmetries, we provide the complete global phase portrait of system (1) in G. The phase portrait shows that the final evolution of the orbital direction of system (1) within G tends to the center of the Poincaré ball as well as the infinite equilibrium points u_{14} and U_{13} located at the waist and equator of the Poincaré sphere (except for the initial conditions $s = 0$), respectively. Based on Hořava-Lifshitz gravity in a Friedmann-Lemaître-Robertson-Walker space-time with non-zero curvature and without the cosmological constant term, equations (21) imply that the value of Hubble parameter H is tending to be zero in the cosmological model as time goes on.

Acknowledgments

The first author gratefully acknowledges the support of the National Natural Science Foundation of China (NSFC) through grant Nos.11672259 and 11571301, the China Scholarship Council through grant No.201908320086, the Ministry of Land and Resources Research of China in the Public Interest through grant No.201411007.

The second author gratefully acknowledges the support of the Ministerio de Economía, Industria y Competitividad, Agencia Estatal de Investigación grants MTM2016-77278-P (FEDER) and MDM-2014-0445, the Agència de Gestió d'Ajuts Universitaris i de Recerca grant 2017SGR1617, and the H2020 European Research Council grant MSCA-RISE-2017-777911.

References

[1] P. Hořava, Quantum gravity at a Lifshitz point, *Physical Review D* **79**, 084008, 2009.

[2] E.M.C. Abreu, A.C.R. Mendes, G. Oliveira-Neto et al., Hořava-Lifshitz cosmological models with noncommutative phase space variables, *General Relativity and Gravitation* **51**, 95, 2019.

[3] S. Carloni, E. Elizalde and P.J. Silva, An analysis of the phase space of Hořava-Lifshitz cosmologies. In: S.D. Odintsov, D. Sáez-Gómez and S. Xambó-Descamps (eds) Cosmology, Quantum Vacuum and Zeta Functions, *Springer Proceedings in Physics* **137**, 139-148, Springer-Verlag, Berlin, 2011.

[4] B. Chen, On Hořava-Lifshitz cosmology, *Chinese Physics C* **35** (5), 429-435, 2011.

[5] F.B. Gao and J. Llibre, Global dynamics of the Hořava-Lifshitz cosmological system, *General Relativity and Gravitation*, Accepted, 2019.

[6] X. Gao,Y. Wang, R. Brandenberger and A. Riotto, Cosmological perturbations in Hořava-Lifshitz gravity, *Physical Review D* **81**, 083508, 2010.

[7] G. Leon and C.R. Fadragas, Cosmological dynamical systems: and their applications, Lambert Academic Publishing, GmbH & Co. KG, 2012.

[8] G. Leon and A. Paliathanasis, Extended phase-space analysis of the Hořava-Lifshitz cosmology, *The European Physical Journal C* **79**, 746, 2019.

[9] G. Leon and E.N. Saridakis, Phase-space analysis of Hořava-Lifshitz cosmology, *Journal of Cosmology and Astroparticle Physics* **2009**, 006, 2009.

[10] S. Lepe and J. Saavedra, On Hořava-Lifshitz cosmology, *Astrophysics and Space Science* **350**, 839-843, 2014.

[11] M. Li and Y. Pang, A trouble with Hořava-Lifshitz gravity, *Journal of High Energy Physics* **08**, 015, 2009.

[12] O. Luongo, M. Muccino and H. Quevedo, Kinematic and statistical inconsistencies of Hořava-Lifshitz cosmology, *Physics of the Dark Universe* **25**, 100313, 2019.

[13] N.A. Nilsson and E. Czuchry, Hořava-Lifshitz cosmology in light of new data, *Physics of the Dark Universe* **23**, 100253, 2019.

[14] A. Paliathanasis and G. Leon, Cosmological solutions in Hořava-Lifshitz gravity, arXiv preprint arXiv: 1903.10821, 2019.

[15] E.N. Saridakis, Aspects of Hořava-Lifshitz cosmology, *International Journal of Modern Physics D* **20** (08), 1485-1504, 2011.

[16] A. Tawfik and E. Abou El Dahab, FLRW cosmology with Hořava-Lifshitz gravity: impacts of equations of state, *International Journal of Theoretical Physics* **56** 7, 2122-2139, 2017.

[17] M. Bhattacharjee, Gravitational radiation and black hole formation from gravitational collapse in theories of gravity with broken Lorentz symmetry, Baylor University, *ProQuest Dissertations Publishing* 22585106, 2019.

[18] S. Mukohyama, Hořava-Lifshitz cosmology: a review, *Classical and Quantum Gravity* **27**, 223101, 2010.

[19] T.P. Sotiriou, Hořava-Lifshitz gravity: a status report, *Journal of Physics: Conference Series* **283**, 012034, 2011.

[20] F. Dumortier, J. Llibre and J.C. Artés, Qualitative theory of planar differential systems, Springer-Verlag, Berlin, 2006.

[21] A. Cima and J. Llibre, Bounded polynomial vector fields, *Transactions of the American Mathematical Society* **318**(2), 557-579, 1990.

[22] M.J. Álvarez, A. Ferragut and X. Jarque, A survey on the blow up technique, *International Journal of Bifurcation and Chaos* **21**(11), 3103-3118, 2011.

[1]School of Mathematical Science, Yangzhou University, Yangzhou 225002, China

E-mail: gaofabao@sina.com (Fabao Gao, ORCID 0000-0003-2933-1017)

[2] Departament de Matemàtiques, Universitat Autònoma de Barcelona, Bellaterra 08193, Barcelona, Catalonia, Spain

E-mail: jllibre@mat.uab.cat (Jaume Llibre, ORCID 0000-0002-9511-5999)